Supplementary Data

CD28 and ITK signals regulate autoreactive T cell trafficking

Nitya Jain[1], Bing Miu[1], Jian-kang Jiang[2], Kai K. McKinstry[1], Amanda Prince[1], Susan L Swain[1], Dale L. Greiner[3], Craig J. Thomas[2], Michael J. Sanderson[4], Leslie J Berg[1] & Joonsoo Kang[1]

[1]Department of Pathology, University of Massachusetts Medical School, 55 Lake Avenue North, Worcester, MA 01655, USA. [2]National Institutes of Health, NIH Chemical Genomics Center, 9800 Medical Center Drive, Rockville, MD 20850, USA [3]Program in Molecular Medicine and [4]Microbiology and Physiological Systems, University of Massachusetts Medical School, Worcester, MA 01655 USA.

Supplementary Table 1: Antibody List

Antibody	Clone	Format	Citation
GP38	eBio8.1.1	eFlour660	http://us.ebioscience.com/mouse-podoplanin-antibody-efluor-660-811.htm
CD31	390	eFlour450	http://us.ebioscience.com/mouse-cd31-antibody-efluor-450-390.htm
CD86	PO3.1	PE	http://us.ebioscience.com/mouse-cd86-antibody-pe-po31.htm
CD80	16-10A1	PerCP-Cy5'5	http://www.bdbiosciences.com/ptProduct.jsp?prodId=744039&key=560526&param=search&mterms=true&from=dTable
CD69	H1.2F3	PE/PE-Cy7	http://us.ebioscience.com/mouse-cd69-antibody-pe-h12f3.htm
CD25	PC61	PE-Cy7	http://www.bdbiosciences.com/ptProduct.jsp?prodId=375423&key=552880&param=search&mterms=true&from=dTable
CD3	145-2C11	PerCp-Cy5.5	http://us.ebioscience.com/mouse-cd3e-antibody-percp-cy55-145-2c11.htm
IL17a	ebio17B7	PerCP-Cy5.5	http://us.ebioscience.com/mouse-il-17a-antibody-percp-cy55-ebio17b7.htm
IFNg	XMG1.2	PE-Cy7	http://www.bdbiosciences.com/ptProduct.jsp?prodId=441271&key=557649&param=search&mterms=true&from=dTable
TNFa	MP6-XT22	PE-Cy7	http://www.bdbiosciences.com/ptProduct.jsp?prodId=441237&key=557644&param=search&mterms=true&from=dTable
IL-10	JES6-16E3	PE	http://www.bdbiosciences.com/ptProduct.jsp?prodId=6182&key=554467&param=search&mterms=true&from=dTable
IL-2	JES6-5H4	PE	http://www.bdbiosciences.com/ptProduct.jsp?prodId=6048&key=554428&param=search&mterms=true&from=dTable
IL-4	11B11	APC	http://us.ebioscience.com/mouse-il-4-antibody-apc-11b11.htm
Caspase-8	1G12		http://www.enzolifesciences.com/ALX-804-447/caspase-8-mouse-mab-1g12/
CD4	RM4-5	PerCP-eFlour670	http://us.ebioscience.com/mouse-cd4-antibody-percp-efluor-710-rm4-5.htm
Annexin V		FITC/PE	http://www.bdbiosciences.com/ptProduct.jsp?prodId=12827&key=556419&param=search&mterms=true&from=dTable
Thy1.2	53-2.1	V500	http://www.bdbiosciences.com/ptProduct.jsp?prodId=1278583&key=561616&param=search&mterms=true&from=dTable
Ly5.1	A20	PE/PE-Cy7	http://us.ebioscience.com/mouse-cd451-antibody-pe-cy7-a20.htm
CD8a	53-6.7	APC-Cy7/ PacBlue	http://www.bdbiosciences.com/ptProduct.jsp?prodId=442936&key=557654&param=search&mterms=true&from=dTable
CD44	IM7	eFlour 450	http://us.ebioscience.com/human-mouse-cd44-antibody-efluor-450-im7.htm
CD62L	MEL-14	PE/FITC	http://us.ebioscience.com/mouse-cd62l-l-selectin-antibody-pe-mel-14.htm
TCRb	H57-597	APC-eFlour 780	http://us.ebioscience.com/mouse-tcr-beta-antibody-apc-efluor-780-h57-597.htm
NK1.1	PK136	PE-Cy7	http://www.bdbiosciences.com/ptProduct.jsp?prodId=375407&key=552878&param=search&mterms=true&from=dTable
CCR7	4B12	PE/PE-Cy7	http://us.ebioscience.com/mouse-cd197-ccr7-antibody-pe-4b12.htm
CCR5	C34-3448	PE	http://www.bdbiosciences.com/ptProduct.jsp?prodId=80599&key=CCR5&param=search&mterms=true&from=dTable
CCR9	eBioCW-1.2	PE	http://us.ebioscience.com/mouse-cd199-ccr9-antibody-pe-ebiocw-12.htm
LFA-1a	M17/4	FITC	http://us.ebioscience.com/mouse-cd11a-antibody-fitc-m17-4.htm
CD103	2E7	APC	http://us.ebioscience.com/mouse-cd103-antibody-apc-2e7.htm
A4b7	DATK32	PE	http://us.ebioscience.com/mouse-lpam-1-antibody-pe-datk32.htm
CXCR3	CXCR3-173	PerCP-Cy5'5/APC	http://us.ebioscience.com/mouse-cd183-cxcr3-antibody-percp-cy55-cxcr3-173.htm
FOXP3	FJK-16a	APC	http://us.ebioscience.com/mouse-rat-foxp3-antibody-apc-fjk-16s.htm
Ki67	B56	FITC/PE	http://www.bdbiosciences.com/ptProduct.jsp?prodId=15725&key=556026&param=search&mterms=true&from=dTable

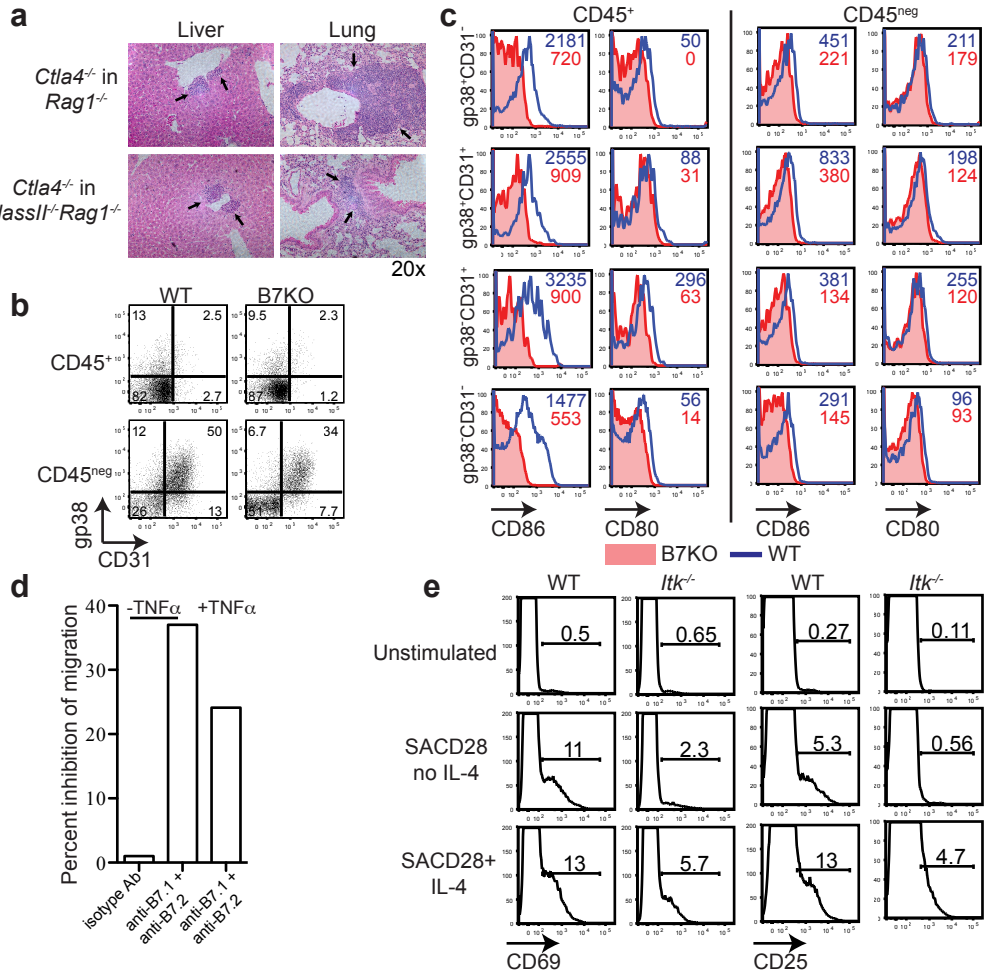

Supplementary Fig. 1: CD28-B7 interactions regulate trans-endothelial T cell migration.

Supplementary Figure 1: CD28–B7 interactions regulate trans–endothelial T cell migration.

a. Representative H&E stained sections of indicated organs from *Rag1*$^{-/-}$ (*n*=7 for histology; *n* =10 total analyzed) and MHC ClassII$^{-/-}$*Rag1*$^{-/-}$ (*n* =4 for histology; *n* =12 total analyzed) mice that had received *Ctla4*$^{-/-}$ cells 6 weeks prior to analysis, respectively. Both *Rag1*$^{-/-}$ and MHC ClassII$^{-/-}$*Rag1*$^{-/-}$ recipients showed infiltration of *Ctla4*$^{-/-}$ T cells into non–lymphoid tissue, as indicated by arrows. **b.** Distribution of stromal cell subsets expressing CD45, gp38 (podoplanin) and CD31 in the lungs of 6–8 weeks old C57/BL6 and *B7*$^{-/-}$ mice was determined after digestion (9ml of 1mg ml^{-1} collagenase Type II + 1ml of 2.5U ml^{-1} Dispase in 1XPBS + 100µl of 1mg ml^{-1} solution of DNase I per gram of tissue) at 37^{o}C for 30 minutes. In the CD45^{neg} compartment, gp38^{+}CD31^{neg} have been identified as follicular reticular cells (FRCs), gp38^{+}CD31^{+} cells as lymphatic endothelial cells (ECs) and gp38^{neg}CD31^{+} cells as blood endothelial cells[1]. The CD45^{neg}gp38^{neg}CD31^{neg} cells are a heterogeneous population of cells including vascular pericytes and other stromal cells[2]. CD45^{+} cells expressing gp38 are follicular dendritic cells[3] and macrophages[4] but may also include CD45^{dim}endothelial cell subsets[5]. **c.** Expression of CD80 and CD86 on different stromal cell compartments shown in **b**: While it is possible that the migratory potential of T cells might be programmed by B7 during their activation in SLOs, this alone cannot account for the aberrant migration of activated *Ctla4*$^{-/-}$ T cells in B7–deficient hosts, given that the T cells were exposed to B7 prior to the transfer. It was therefore likely that functional B7 exists within non–lymphoid tissues. While it is possible that the migratory potential of T cells might be programmed by B7 during their activation in SLOs, this alone cannot account for the aberrant

migration of activated *Ctla4*$^{-/-}$ T cells in B7–deficient hosts, given that the T cells were exposed to B7 prior to the transfer. It was therefore likely that functional B7 exists within non–lymphoid tissues. While there was moderate amount of CD86 expression on CD45^{+} hematopoietic cell subsets, CD45^{neg} stromal cell subsets expressed relatively low amounts of CD86. B7–deficient cells were used as negative staining controls (red filed histograms). Numbers in the plots indicate median fluorescent intensities. Data are representative of 3 independent experiments with 2 mice in each group. **d.** Percent inhibition of migration of *Ctla4*$^{-/-}$ T cells across TNF–α stimulated and un–stimulated ECs (SVEC4–10 cell system; model system to study chemokine, adhesion and costimulatory molecule–regulated diapedesis) by anti–B7.1 and anti–B7.2 antibodies compared to isotype antibody. EC monolayer on trans–well insert was pre–treated with B7 antibodies for 2 hours prior to the migration assay. Data are representative of 4 experiments with at least 4 replicates in each experiment. **e.** Sorted naïve (CD44^{-} CD62L^{+}) CD4^{+} cells from WT and *Itk*$^{-/-}$ mice were stimulated at 37^{o}C with CD28 superagonist antibody (SACD28) (10μg ml^{-1}) ± rIL–4 (2ng ml^{-1}). Expression of early activation markers CD25 and CD69 were determined on live CD4^{+} T cells after 24 hours of activation. Data are representative of 3 independent experiments. Activation using strong agonists (anti CD3 and CD28 antibody crosslinking) resulted in substantially higher expression of both markers (>50% positive; data not shown).

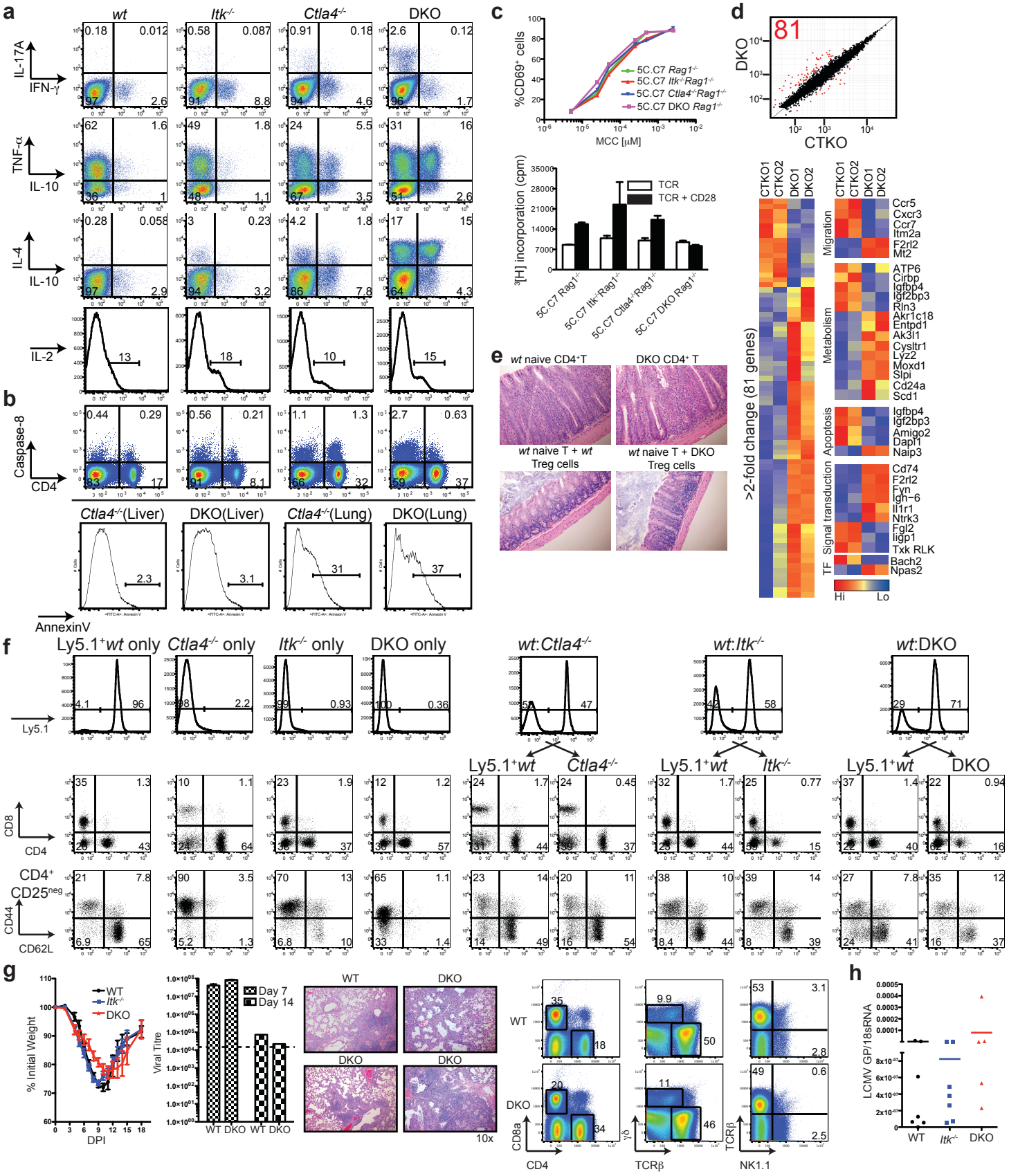

Supplementary Fig. 2: Phenotypic and molecular characterization of DKO CD4⁺ T cells.

Supplementary Fig. 2: Phenotypic and molecular characterization of DKO CD4$^+$ T cells.

CD28 signaling is necessary for the activation of self–reactive *Ctla4*$^{-/-}$ T cells *in vivo*[6]. While altering specific downstream mediators of CD28 in *Ctla4*$^{-/-}$ mice was predicted to reveal pathways that contribute to the pathogenesis of T cell mediated autoimmunity, the challenge was to identify components that have biased function in specific facets of CD28–mediated disease pathogenesis. ITK was an ideal candidate, since the loss–of–function of ITK does not completely abolish TCR–CD28 signaling, but primarily impairs the PI3K–PLCγ1 pathway[7]. Consequently, naïve DKO CD4$^+$ T cells respond to their cognate antigens comparably to WT T cells, and DKO mice are replete with activated T cells; these findings established that the CD28 costimulatory signals necessary for the initial activation of *Ctla4*$^{-/-}$ T cells are intact in the absence of ITK. Further, DKO mice are effective in pathogen clearance, again confirming that T cell activation and differentiation are not globally impaired. Hence, the inability of activated DKO T cells to enter tissues and to cause fatal autoimmunity revealed a specific function of ITK in self–reactive T cell trafficking.

a. CD4$^+$ T cells from the LNs of 8 weeks old WT, *Itk*$^{-/-}$ and DKO mice and 3 weeks old *Ctla4*$^{-/-}$ mice were tested for their ability to make effector cytokines following 4 hour *ex vivo* stimulation with PMA and Ionomycin in the presence of Golgi inhibitors. Representative FACS profiles for intra–cellular staining for IL–17A, IFN–γ, TNF–α, IL–10, IL–4 and IL–2 on CD4$^+$T cells are shown. Data are representative of at least 3 independent experiments with 2 mice in each group. While 8 weeks old DKO T cells consistently produced more IL–4 and IL–10 compared to much younger and sick *Ctla4*$^{-/-}$

mice, the difference was not dramatic when 3 weeks old DKO mice were compared. **b.** (*Top*) Expression of the cell death marker Caspase–8 on $CD4^+$T cells from 8 weeks old WT, *Itk*$^{-/-}$ and DKO mice and 3 weeks old *Ctla4*$^{-/-}$ mice. (*Bottom*) Annexin V staining of $Thy1.2^+CD4^+$ T cells in the liver and lungs of 3 weeks old *Ctla4*$^{-/-}$ and 6 months old DKO mice. Older DKO mice were used to obtain sufficient numbers of T cells for analysis. Data are representative of 2 experiments with 3–4 mice per group. **c.** 5C.C7*Itk*$^{-/-}$ *Rag1*$^{-/-}$ mice were crossed with 5C.C7*Ctla4*$^{-/-}$*Rag1*$^{-/-}$ mice to generate 5C.C7DKO*Rag1*$^{-/-}$ mice. Naïve $CD4^+$T cells were activated with indicated concentrations of moth cytochrome c peptide (MCC) pulsed I–E^k expressing CHO cells. (*Top*) Frequency of T cells expressing the early activation marker CD69 at 24 hours post–activation. (*Bottom*) Proliferation of T cells activated with $5e^{-4}$μM of MCC was measured by tritiated Thymidine uptake assay. Data are representative of 2 independent experiments. Error bars are standard error of means. **d.** Global gene expression profiling of $CD4^+CD25^{neg}$ T cells from 3 weeks old *Ctla4*$^{-/-}$ and DKO mice was performed using an Affymetrix MoGene 1.0 ST array. (*Top*) Scatter plot showing differential expression of genes between *Ctla4*$^{-/-}$ (CTKO) and DKO mice. Each dot represents one gene (mean of all probe sets) and red indicates genes with expression change of more than two–fold. Of the 17,552 annotated genes with expression values greater than 120 in at least one subset (classified as expressed genes), 81 genes were changed in expression by greater than 2–fold between *Ctla4*$^{-/-}$ and DKO mice. *(Bottom*). Heat maps of expression of genes with greater than 2–fold change overall (*Left*) and segregated based on indicated biological processes (*Right*). Each column represents individual samples of indicated genotype. All data were log transformed and row normalized for display. 12/81 differentially expressed

genes were Ig transcripts that were higher in DKO samples, possibly due to a downregulation of *Bach2* in DKO T cells, and are not likely to be functionally relevant for T cells. **e.** Similar to *Ctla4*$^{-/-}$ mice, DKO mice exhibited an increased frequency of FOXP3^{+} Treg cells in peripheral SLOs, but the Treg cells were functionally compromised. Representative H&E stained sections of colons from indicated mouse groups 6 weeks after adoptive transfer of naïve CD4^{+} T cells with WT or DKO Treg cells. Transmural inflammation and pathology in recipients of naïve WT cells and DKO CD4^{+}CD25^{neg} cells alone was observed. Co–transfer of WT Treg cells prevented the development of colitis by WT naïve cells, while DKO Treg cells failed to do so. However, the degree of colonic pathology was decreased in the presence of DKO Treg cells, suggesting that, similar to *Ctla4*$^{-/-}$ Treg cells[8], DKO Treg cells might retain some functionality in this assay of Treg cell function. Data are representative of 2 experiments with 4 mice in each group. **f.** (*Top*) *Rag1*$^{-/-}$ mice reconstituted with BM from Ly5.1^{+}WT, Ly5.2^{+}*Ctla4*$^{-/-}$, Ly5.2^{+}*Itk*$^{-/-}$ and Ly5.2^{+}DKO mice. (*Bottom*) *Rag1*$^{-/-}$ mice reconstituted with a 1:1 mix of BM from Ly5.1^{+}WT and Ly5.2^{+}*Ctla4*$^{-/-}$ mice, Ly5.1^{+}WT and Ly5.2^{+}*Itk*$^{-/-}$ mice or Ly5.1^{+}WT and Ly5.2^{+}DKO mice. The frequency of CD4^{+} and CD8^{+} T cells and frequency of activated CD44^{hi}CD62L^{lo} CD4^{+}CD25^{neg} T cells in the spleen was determined by flow cytometry at 8 weeks post reconstitution. Data are representative of 2 independent experiments with 5 mice in each group. **g.** (From *left* to *right*) Body weights of the A/PR8 Influenza A virus infected mice at indicated days post–infection (DPI); Lung viral titers were determined at d7 and d14 post–infection (dashed line represents the limit of detection); Representative H&E stained sections of lungs from 1 WT and 3 DKO mice 22 days post–infection; Representative flow cytometry dot plots showing frequency of various T cell subsets in

lungs of infected WT and DKO mice. These data indicate that DKO mice clear Flu virus with similar kinetics as WT mice. Further, contrary to the lack of migration of autoreactive DKO T cells in uninfected mice, virus–induced effector T cells in infected DKO mice migrated efficiently to lung tissues. **h.** qPCR analysis of LCMV glycoprotein expression in spleens from d11 infected mice showed no significant differences in viral clearance between WT and DKO mice. Data in **g** and **h** are representative of 2 independent experiments for each virus infection.

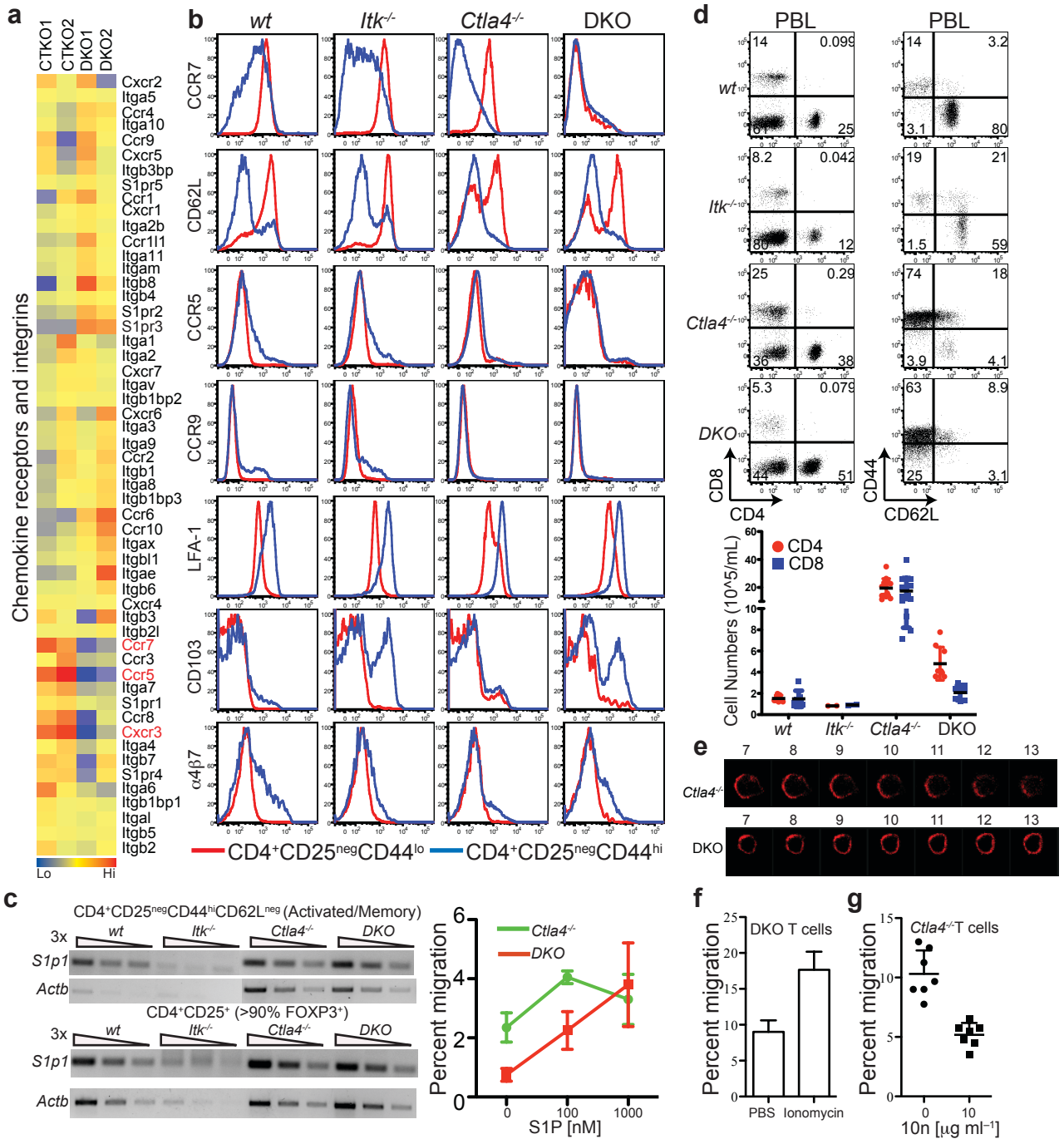

Supplementary Fig. 3: Similar pattern of chemokine receptor and integrin expression on DKO and *Ctla4*$^{-/-}$ CD4^{+} T cells

Supplementary Fig. 3: Similar pattern of chemokine receptor and integrin expression on DKO and *Ctla4*$^{-/-}$ CD4^{+} T cells

a. A heat map of gene expression of chemokine receptors and integrins in CD4^{+}CD25^{neg} T cells from *Ctla4*$^{-/-}$ (CTKO) and DKO mice. Data were log transformed and row normalized for display. Each column represents individual samples of indicated genotype. While transcripts for *Ccr5* and *Ccr7* were reduced in DKO T cells, protein expression analysis by flow cytometry (**b**) did not show significant differences to activated (CD44^{+}) *Ctla4*$^{-/-}$ conventional CD4^{+} T cells (Tconv, FOXP3^{neg}) for CCR7 and only a marginal difference in MFI for CCR5. Further, DKO and *Ctla4*$^{-/-}$ T cells migrated similarly to chemokine CCL5, a ligand for CCR5 (data not shown), suggesting that these pathways were not relevant in the impaired migration of DKO T cells *in vivo*. **b.** LN cells from 6–8 weeks old WT, *Itk*$^{-/-}$ and DKO mice and 3 weeks old *Ctla4*$^{-/-}$ mice were analyzed for the cell surface expression of various chemokine receptors and integrins. Representative flow cytometric histograms showing expression of CCR7, CD62L, CCR5, CCR9, LFA–1, CD103 and α4β7 on CD4^{+}CD25^{neg}CD44^{lo} (red) and CD4^{+}CD25^{neg}CD44^{hi} (blue) T cells. Low CCR7 expression on CD44^{lo} DKO CD4^{+} T cells relative to those from *Ctla4*$^{-/-}$ mice reflects a near absence of CD44^{-}CD62L^{+} naïve T cells in 6 weeks old DKO mice (**Fig. 2c**). Data are representative of 2 independent experiments with 2–3 mice in each group. **c.** (*Left*) Semi–quantitative RT–PCR analysis of expression of S1P1 relative to β–actin in CD4^{+}CD25^{neg}CD44^{hi}CD62L^{lo} (activated Tconv) and CD4^{+}CD25^{+} (Treg) cells from WT, *Itk*$^{-/-}$, *Ctla4*$^{-/-}$ and DKO mice. (*Right*) Trans–well migration assay showing frequency of migration of CD4^{+}T cells from *Ctla4*$^{-/-}$ and DKO mice to different concentrations of S1P ligand. Data are representative of 3 independent experiments **d.** (*Left*) Frequency of CD4^{+}

and $CD8^+$ T cells in peripheral blood lymphocytes (PBL) and (*Right*) expression of the activation markers CD44 and CD62L (L–Selectin) on blood $CD4^+CD25^{neg}$ T cells of 6–8 weeks old WT, $Itk^{-/-}$ and DKO mice and 3 weeks old $Ctla4^{-/-}$ mice. (*Bottom*) Numbers of $CD4^+$ and $CD8^+$ lymphocytes in peripheral blood of 3 weeks old WT, $Itk^{-/-}$, $Ctla4^{-/-}$ and DKO mice. **e.** F–actin staining of purified $CD4^+$ T cells from 3 weeks old $Ctla4^{-/-}$ and 8 weeks old DKO mice. Representative serial *z*–stacks of a single lymphocyte from $Ctla4^{-/-}$ and DKO mice are shown. >85% of $CD4^+$T cells had an activated $CD44^{hi}CD62L^{lo}$ phenotype from both $Ctla4^{-/-}$ and DKO mice prior to staining. **f.** DKO LN cells were stimulated with the Ca^{2+} ionophore, Ionomycin (2μg ml^{-1}) for 2 hours prior to a trans–endothelial migration assay. Plot shows frequency of DKO cells stimulated with Ionomycin or left untreated (in saline) migrating across SVEC4–10 cells after 4 hours. Data are representative of 3 independent experiments with 4–5 replicates in each experiment. **g.** $CD4^+$ T cells from $Ctla4^{-/-}$ mice were pre–treated for 2 hours with the ITK inhibitor 10n (10μg ml^{-1}) prior to a trans–endothelial migration assay Error bars are standard error of means. Data are representative of at least 2 independent experiments with 3–4 replicates for each condition.

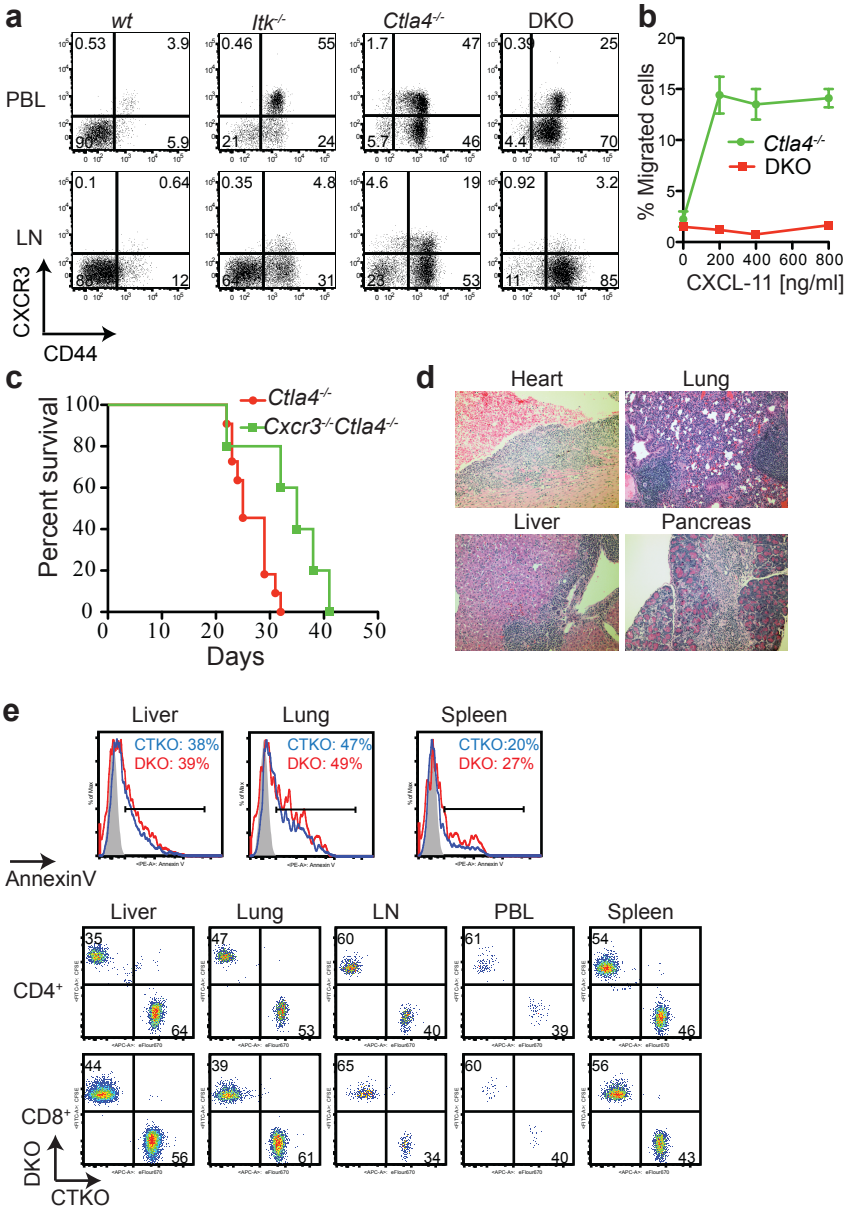

Supplementary Fig. 4: Tissue homing defects of DKO T cells cannot be solely accounted for by alterations in CXCR3 expression and function

Supplementary Fig. 4: Tissue homing defects of DKO T cells cannot be solely accounted for by alterations in CXCR3 expression and function

a. Expression of the chemokine receptor, CXCR3, and activation marker CD44 on $CD4^+CD25^{neg}$ Tconv cells in peripheral blood and LNs of 8 weeks old WT, *Itk*$^{-/-}$ and DKO mice and 3 weeks old *Ctla4*$^{-/-}$ mice. **b.** Frequency of migration of $CD4^+$T cells from *Ctla4*$^{-/-}$ and DKO mice to indicated concentrations of the CXCR3 ligand CXCL–11 in vitro. **c.** Kaplan–Meier survival curves of *Ctla4*$^{-/-}$ (n=10) and *Cxcr3*$^{-/-}$*Ctla4*$^{-/-}$ (n=5) mice show an approximate 10–day extension in the lifespan of the latter. **d.** Representative H&E stained sections from indicated organs of 3–4 weeks old *Cxcr3*$^{-/-}$ *Ctla4*$^{-/-}$ mice show massive infiltration into non–lymphoid tissue by *Cxcr3*$^{-/-}$*Ctla4*$^{-/-}$ T cells, indicating that decreased CXCR3 expression alone cannot account for the lack of infiltration and autoimmunity in *Itk*$^{-/-}$*Ctla4*$^{-/-}$ DKO mice. **e.** (*Top*) Representative histogram overlays showing similar AnnexinV staining on *Ctla4*$^{-/-}$ (blue) and DKO (red) $CD4^+$ T cells isolated from the liver, lungs and spleen of *Rag1*$^{-/-}$ mice that had received a mix of eFluor670–labeled *Ctla4*$^{-/-}$ T cells and CFSE–labeled DKO T cells 6–8 hours prior to analysis. Gray shaded histograms are the unstained controls. (*Bottom*) Representative dot plots show distribution of eFluor670–labeled *Ctla4*$^{-/-}$ and CFSE–labeled DKO $CD4^+$ and $CD8^+$ T cells in the liver, lungs, lymph nodes (LN), peripheral blood and spleen of *Rag1*$^{-/-}$ mice that had received a 1:2 mix of *Ctla4*$^{-/-}$ and DKO T cells 6–8 hours prior to analysis. There is a lower frequency of DKO T cells relative to *Ctla4*$^{-/-}$ T cells in non–lymphoid tissues. This disparity is most likely an underestimate since at the time of T cell isolation for transfer, most T cells in DKO mice reside in lymphoid tissues, whereas *Ctla4*$^{-/-}$ T cells are replete in most non–lymphoid tissues.

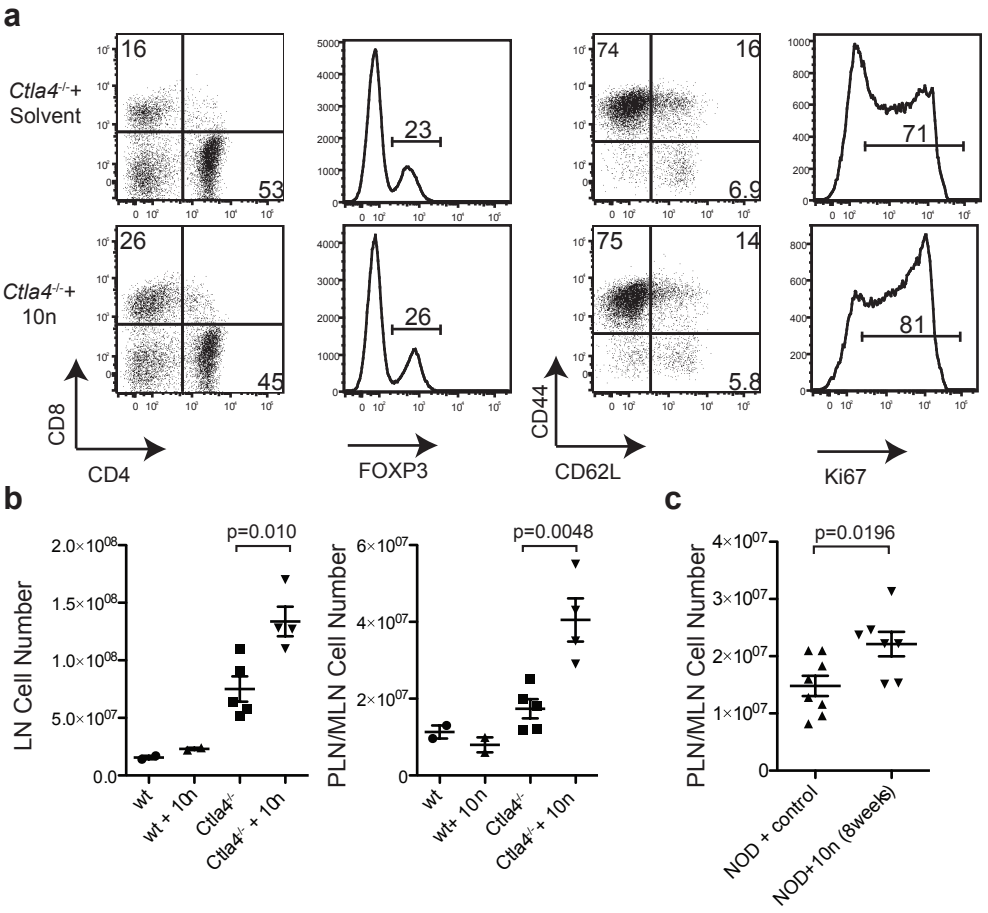

Supplementary Fig. 5: ITK inhibitor treatment does not alter activation of auto-reactive T cells but affects trafficking *in vivo*.

Supplementary Fig. 5: ITK inhibitor treatment does not alter activation of auto–reactive T cells but affects trafficking *in vivo*.

a. Frequency of $CD4^+$, $CD8^+$ and $CD4^+FOXP3^+$ T cells in peripheral LNs of *Ctla4*$^{-/-}$ mice treated with solvent or ITK inhibitor at 3.5 weeks of age. $CD4^+FOXP3^{neg}$ Tconv cells were further analyzed for the expression of activation markers, CD44 and CD62L, and proliferation marker, Ki67. Data are representative of 2 independent experiments with 2 mice in each group. **b.** Cellularity of peripheral LNs (*Left*) and pooled mesenteric and pancreatic LNs (*Right*) of 3.5 weeks old WT and *Ctla4*$^{-/-}$ mice treated with the ITK inhibitor 10n. Data are pooled from 2 experiments with at least 2 mice in each group. **c.** Cellularity of pooled mesenteric and pancreatic LNs from 8 weeks old female NOD mice treated with the ITK inhibitor 10n or solvent alone. Data are pooled from 2 experiments with at least 3 mice in each group.

Supplementary Movie 1: *Ctla4*$^{-/-}$ T cells are highly motile in blood vessels of lung slices from *B7*$^{+/+}$ mice.

CFSE labeled *Ctla4*$^{-/-}$ T cells (pseudo-labeled green) were intravenously injected into *B7*$^{+/+}$ mice that were previously injected with CMTMR Orange dye (pseudo-labeled red). An average of 16 frames per second was captured every 5 seconds using Video Savant software and a QuickTime movie rendition was made at 30 frames/second. The movie shows movement of *Ctla4*$^{-/-}$ T cells along blood vessel walls with characteristically elongated migratory morphology along vessel walls. One *Ctla4*$^{-/-}$ T cell is also shown crossing the endothelial barrier.

Supplementary Movie 2: *Ctla4*$^{-/-}$ T cells lose characteristic morphology and motility in blood vessels of lung slices from B7-deficient mice.

CFSE labeled *Ctla4*$^{-/-}$ T cells (pseudo-labeled green) were intravenously injected into *Cd80*$^{-/-}$*Cd86*$^{-/-}$ mice that were previously injected with CMTMR Orange dye (pseudo-labeled red). An average of 16 frames per second was captured every 5 seconds using Video Savant software and a QuickTime movie rendition was made at 30 frames/second. The movie shows the altered morphology and migratory behavior of *Ctla4*$^{-/-}$ T cells in vessel of B7-deficient mice. *Ctla4*$^{-/-}$ T cells become rounded and display random motility in the absence of B7, as opposed to directional movement in B7-sufficient lung slices.

Supplementary Movie 3: *Ctla4*$^{-/-}$ T cells are highly motile in blood vessels of lung slices from *Rag1*$^{-/-}$ mice.

CFSE labeled *Ctla4*$^{-/-}$ T cells (pseudo-labeled green) were intravenously injected into

Rag1$^{-/-}$ mice that were previously injected with CMTMR Orange dye (pseudo-labeled red). An average of 16 frames per second was captured every 5 seconds using Video Savant software and a QuickTime movie rendition was made at 30 frames/second. The movie shows movement of *Ctla4*$^{-/-}$ T cells with characteristically elongated migratory morphology along vessel walls; some T cells are shown moving across the endothelial cell layer into tissues, while 1 *Ctla4*$^{-/-}$ T cell is stationery at the vessel wall. The behavior of *Ctla4*$^{-/-}$ T cells in RAG-1-deficient mice is similar to that seen in B7-sufficient RAG-1-sufficient mice (**Supplementary Movie 1**)

Supplementary Movie 4: DKO T cells do not show migratory behavior in blood vessels of lung slices.

CFSE labeled DKO T cells (pseudo-labeled green) were intravenously injected into *Rag*$^{-/-}$ mice that were previously injected with CMTMR Orange dye (pseudo-labeled red). An average of 16 frames per second was captured every 5 seconds using Video Savant software and a QuickTime movie rendition was made at 30 frames/second. The movie shows the behavior of DKO T cells within blood vessel of lung slices; unlike *Ctla4*$^{-/-}$ T cells, DKO T cells are rounded and do not make stable contacts with vessel walls. They do not display directionality in movement, have random motility and do not get across the endothelial barrier.

References:

1. Fletcher, A.L.*, et al.* Lymph node fibroblastic reticular cells directly present peripheral tissue antigen under steady-state and inflammatory conditions. *The J Exp Med.* **207**, 689-697 (2010).
2. Malhotra, D.*, et al.* Transcriptional profiling of stroma from inflamed and resting lymph nodes defines immunological hallmarks. *Nat Immunol.* **13**, 499-510 (2012).
3. Yu, H., Gibson, J.A., Pinkus, G.S. & Hornick, J.L. Podoplanin (D2-40) is a novel marker for follicular dendritic cell tumors. *Am J Clin Pathol. 1***28**, 776-782 (2007).
4. Hou, T.Z.*, et al.* A distinct subset of podoplanin (gp38) expressing F4/80+ macrophages mediate phagocytosis and are induced following zymosan peritonitis. *FEBS Lett.* **584**, 3955-3961 (2010).
5. Bertolini, F., Shaked, Y., Mancuso, P. & Kerbel, R.S. The multifaceted circulating endothelial cell in cancer: towards marker and target identification. *Nat Rev Cancer.* **6**, 835-845 (2006).
6. Mandelbrot, D.A.*, et al.* B7-dependent T-cell costimulation in mice lacking CD28 and CTLA4. *J Clin Invest.* **107**, 881-887. (2001).
7. Berg, L.J., Finkelstein, L.D., Lucas, J.A. & Schwartzberg, P.L. Tec family kinases in T lymphocyte development and function. *Ann Rev Immunol.* **23**, 549-600 (2005).
8. Read, S.*, et al.* Blockade of CTLA-4 on CD4+CD25+ regulatory T cells abrogates their function in vivo. *J Immunol.* **177**, 4376-4383 (2006).